Herráez, M., Mora, D., Naya, F., Lopes, C. S., González, C. & LLorca, J. (2015). Transverse cracking of cross-ply laminates: A computational micromechanics perspective. *Composites Science and Technology, 110*, 196–204.

DOI: 10.1016/j.compscitech.2015.02.008

Transverse cracking of cross-ply laminates: a computational micromechanics perspective

Miguel Herráez[a], Diego Mora[a], Fernando Naya[a], Claudio S. Lopes[a], Carlos González[a,b], Javier LLorca[a,b,*]

[a] *IMDEA Materials Institute, C/Eric Kandel 2, 28906 Getafe, Madrid, Spain*

[b] *Department of Materials Science, Polytechnic University of Madrid, 28040 Madrid, Spain*

Abstract

Transverse cracking in cross-ply carbon/epoxy and glass/epoxy laminates in tension is analyzed by means of computational micromechanics. Longitudinal plies were modeled as homogenized, anisotropic elastic solids while the actual fiber distribution was included in the transverse plies. The mechanical response was obtained by the finite element analysis of a long representative volume element of the laminate. Damage in the transverse plies was triggered by interface decohesion and matrix cracking. The simulation strategy was applied to study the influence of ply thickness on the critical stress for the cracking of the transverse plies and on the evolution of crack density in $[0^\circ_2/90^\circ_{n/2}]_s$ laminates, with $n = 1$, 2, 4 and 8. It was found that the transverse ply strength corresponding to the initiation and propagation of a through-thickness crack was independent of the ply thickness and that the transverse strength of carbon/epoxy laminates was 35% higher than that of the glass fiber counterparts. In addition, the mechanisms of crack initiation and propagation through the thickness as well as of multiple matrix cracking were ascertained and the stiffness reduction in the 90° ply as a function of crack density was computed as a function of the ply thickness.

*Corresponding author

Email address: javier.llorca@imdea.org (Javier LLorca)

February 12, 2015

Keywords: A. polymer-matrix composites (PMC's), C. Finite element analysis, C. Transverse cracking, C. Computational mechanics

1. Introduction.

Fiber-reinforced polymers are nowadays extensively used in engineering applications which require high specific stiffness and strength. They present several different physical failure mechanisms and transverse ply cracking (also denominated matrix cracking) is very often the first one to develop under the application of thermal or mechanical loads. Nucleation and propagation of matrix cracks do not normally lead to structural collapse but degrades very rapidly the laminate resistance to permeation and leakage, limiting the application of cracked laminates in pressure vessels, fuel tanks, etc. Moreover, transverse ply cracks induce interply delamination which may have more serious consequences from the structural viewpoint.

The mechanics of matrix cracking is now well established on the basis of extensive experimental campaigns and of analytical models. The first microcrack causes negligible changes in the thermo-mechanical response of the laminate, but the crack density (the number of cracks per unit length) increases with the applied strain until saturation, leading to material degradation in terms of a moderate to significant loss in the ply transverse stiffness and shear modulus. Extensive reviews of matrix cracking and its effect on the behavior of composite laminates are available in the works of Nairn [1] and Talreja and Singh [2].

The onset of matrix cracking and the crack density at saturation is dictated by a number of factors, including the quality of the material (which is controlled by fiber distribution as well as by the mechanical properties of the matrix and of the fiber/matrix interface) together with the laminate stacking sequence and thickness [1]. Parvizi *et al.* [3, 4] studied the influence of the ply thickness on the strain-to-failure of the 90° layers on glass-epoxy cross-ply cross-ply $[0/90]_s$ laminates by varying the relative thickness of the inner 90° layers with respect to the supporting 0° plies. They found that the thinner the internal layers, the higher the critical strain for crack initiation and the crack density. For sufficiently thin inner plies, matrix cracking could eventually be suppressed prior to the failure of the supporting layers which

determines the final collapse of the specimen. In addition, the position of the 90° layers relative to the supporting plies also influences the critical strain and Nairn [1] showed that matrix cracking occurs at early stages in $[90/0]_s$ laminates, due to the lack of constrain on the external plies. Similar trends were reported in [5, 6] for $[\pm\theta/90°]_s$ carbon-epoxy laminates, with different θ values. To take advantage of this phenomenon, Kawabe *et al.* [7] developed the tow-spreading technique which can be used to produce prepreg tapes with a thickness below one-third of that of conventional laminates, leading to thin ply laminates which present outstanding damage tolerance [8, 9].

The mechanics of transverse matrix cracking in cross-ply laminates was analyzed by Dvorak and Laws [10] from a fracture mechanics perspective. They assumed the presence of an initial crack nucleus and computed the energy release rate for the crack propagation through the ply thickness and parallel to the fibers. Crack propagation occurs when the energy release rate is equal to the fracture energy G_c. In the case of uniaxial tension perpendicular to the fibers, the critical stress that leads to the through-thickness crack propagation, Y_T^{tt}, is given by

$$Y_T^{tt} = \sqrt{\frac{2G_c}{\pi\delta_c\Lambda_{22}}} \tag{1}$$

where δ_c is the crack length in the through-the-thickness direction ($<< t$, the ply thickness) and $\Lambda_{22} = 2(1/E_1 - \nu_{12}^2/E_2)$ where E_1, E_2 and ν_{12} stand for the longitudinal and transverse elastic modulus of the ply and the in-plane Poisson's ratio, respectively. Dvorak and Laws [10] assumed that the initial crack nucleus was controlled by the microstructural inhomogeneities in the composite and thus Y_T^{tt} was independent of the ply thickness.

The energy release rate for through-thickness propagation remains greater than the energy release rate for propagation parallel to the fibers (tunneling) until the crack approaches the interface. Assuming that the through-thickness crack has spanned the whole ply thickness, the critical stress for the continuation of crack propagation along the fibers, Y_T^l, under uniaxial tension perpendicular to the fibers is given by

$$Y_T^l = \sqrt{\frac{8G_c}{\pi t \psi_I}} \tag{2}$$

where ψ_I is a coefficient (of the order of the unity) that takes into account the constraint of the adjacent plies [11]. Transverse ply cracking requires an applied tensile stress higher than both Y_T^{tt} and Y_T^l. Whether $Y_T^{tt} > Y_T^l$ or *vice versa* depends on the size of the initial crack nucleus, δ_c and on the ply thickness t but it is evident that the transverse cracking stress is given by equation (1) in very thick plies. As the δ_c is unknown, Dvorak and Laws [10] related the *in situ* transverse strength of thick plies to the transverse tensile strength measured on an unconstrained unidirectional ply, Y_T, as:

$$Y_T^{tt} = 1.12\sqrt{2}Y_T \tag{3}$$

where the factor 1.12 accounts for the stress intensity magnification of a surface crack. In the case of very thin plies, the transverse strength was given by equation (2) and it was proportional to $1/\sqrt{t}$.

These predictions for the behavior of thick and thin plies were in good agreement with the experimental observations [3, 5, 6] but the model was not able to predict the critical ply thickness that separates "thin" from "thick" plies because δ_c is unknown. Moreover, the actual value of the critical stress for crack initiation, Y_T^{tt} in equation (1), cannot be predicted because is a function of the unknown size of the initial crack nucleus, while the validity of the *in situ* ply strength in equation (3) has not been ascertained [12]. Nevertheless, these limitations can be overcome by means of computational micromechanics, which can account for the influence of matrix, fiber and interface properties on the onset and development of matrix cracking. Computational micromechanics is emerging in recent years as a powerful tool to predict the influence of the constituent properties on the ply behavior under different loading conditions, including transverse compression [13], shear [14] and fracture [15, 16, 17]. This information can be used as input in multiscale modeling strategies aimed at predicting the laminate and component behavior [18]. Computational micromechanics is used here to analyze the effect of ply thickness on the onset and development of transverse ply cracking in cross-ply carbon/epoxy and glass/epoxy laminates.

2. Computational micromechanics strategy

The onset and development of transverse matrix cracking in cross-ply $[0_2/90_{n/2}]_s$ laminates was studied by means of the finite element analysis of a representative volume element of the material (RVE). The RVE is rectangular with length $L = 10$ mm and thickness t=2($\frac{n}{2}$+2)t_0 where t_0 is the thickness of a single ply, Figure 1(a). t_0 was equal to 68.75 μm in the case of glass fiber composites and to 34.38 μm in the case of carbon fiber composites to account for the smaller radius of carbon fibers. The length of the RVE was long enough to compute accurately the increment in crack density upon deformation along the x direction. Obviously, this 2D model can only account for the through-thickness initiation and propagation of cracks. Simulation of crack tunneling will require a full 3D simulation which is out of the scope of this paper.

The 0° plies were assumed to be homogenized, transversally isotropic elastic solids, with equivalent effective properties, while the actual random fiber spatial distribution was included in the 90° ply (Figure 1(b). The fiber radius was constant and equal to $R = 9$ μm for E glass fibers and to 4.5 μm for AS4 carbon fibers and the fibers were dispersed in the 90° ply using the modified random sequential adsorption algorithm [19]. This algorithm provides random fiber distribution within the RVE while imposing some limitations on the minimum distance between the fiber surfaces ($> 0.07R$) and between the fiber surface and the ply edges ($> 0.1R$) to avoid the presence of distorted finite element during meshing. The fiber volume fraction within the RVE was set to 65%. It should be indicated that the fibers intersecting the internal edges with the 90° plies were removed from the model to represent the typical matrix rich region between adjacent plies with different angle directions, Figure 1(b), but it was ensured that the final volume fraction was always 65%. The RVE was discretized with generalized plain strain isoparametric four-noded quadrilateral elements (CPEG4 in Abaqus/Standard [20]). Special care was taken to obtain a good mesh discretization between fiber ligaments, as this is necessary to capture adequately the complex stress gradients in these regions, Figure 1(c). In addition, four-noded isoparametric cohesive elements (COH2D4 in Abaqus/ Standard [20]) with thickness of $10^{-3}\mu$m) were inserted at the fiber/matrix interfaces to address interface decohesion during the simulations.

Four different RVEs were generated, corresponding to $n = 1$, 2, 4 and 8, to analyze the influence of ply thickness on the mechanics of matrix cracking. The fiber distribution in a central slice of the RVE is shown in Figure 2 for the different RVEs. The total length of the RVEs is always 10 mm along the x axis (not included in Figure 2) while the thickness of the central 90° ply is nt_0.

Periodic boundary conditions were applied to the edges of the RVE to maintain the continuity between adjacent RVE's. They can be expressed as:

$$\begin{aligned} \vec{u}(0,z) - \vec{\delta_x} &= \vec{u}(L,z) \\ \vec{u}(x,-t/2) - \vec{\delta_z} &= \vec{u}(x,t/2) \end{aligned} \tag{4}$$

where $\vec{\delta_x} = (\delta_x, 0)$ stands for the imposed displacement vector along the x direction and $\vec{\delta_z} = (0, \delta_z)$ is computed from the condition that the average stresses along the through-the-thickness direction should be zero, the plane stress condition in the $x - y$ plane of the laminate [19].

The properties of the E glass and AS4 carbon fibers were taken from the literature [17, 21]. E-glass fibers were considered as isotropic, thermo-elastic solids with elastic modulus E_f =74 GPa, Poisson's ratio $\nu_f = 0.2$ and coefficient of thermal expansion α_f=$10^{-5}\mathrm{K}^{-1}$. AS4 carbon fibers were transversally isotropic elastic solids, with elastic moduli $E_{f1} = 232$ GPa and $E_{f2} = 13$ GPa in the fiber and transverse directions, respectively, in plane and out-of-plane Poisson's ratios $\nu_{f12} = 0.3$ and $\nu_{f23} = 0.46$, respectively, and in plane and out-of-plane shear moduli, $G_{f12} = 11.3$ GPa and $G_{f23} = 4.45$ GPa, respectively. The coefficients of thermal expansion of AS4 carbon fiber in the longitudinal and transverse directions were, respectively, $\alpha_{f1} =$ -0.9 $10^{-6}\mathrm{K}^{-1}$ and $\alpha_{f2} = 7.2\ 10^{-6}\mathrm{K}^{-1}$.

The properties of the epoxy matrices for the composites reinforced with carbon or glass fibers were also taken from the literature. Those of the carbon fiber composite are characteristic of a Hexply resin 8552 from Hexcel [22] while those of the glass fiber composite correspond to an MTM57 resin from the Advanced Composite Group [17]. The epoxy matrices were modelled as isotropic, elasto-plastic solids, with thermo-elastic constants E_m, ν_m, and α_m. Plastic deformation and damage was accounted for by means of a continuum plasticity-damage model proposed by Lee and Fenves [23] based on a previ-

ous model developed by Lubliner [24]. The model, schematically described in Figure 3, takes into account the pressure-sensitivity of the epoxy flow stress under compression and its brittle behavior in tension, and has been successfully applied to analyze intraply crack propagation in glass fiber-reinforced polymers [17]. Under compression, the matrix follows the standard Drucker-Prager yield criterion, which is determined by the compressive flow stress, σ_m^c and the pressure sensitivity parameter, α_{ps}. The mechanical behavior of the matrix in tension is brittle and the tensile strength of the matrix is σ_m^t. The post-peak behavior is controlled by a softening law characterized by the matrix fracture energy G_m. The actual values of the parameters that characterize the matrix behavior can be found in Table 5. More details about the constitutive model and the numerical implementation can be found in [17, 20]

The fiber-matrix interface was modeled as a cohesive crack, whose mechanical behavior is expressed in terms of a bilinear traction-separation law which relates the displacement jump across the interface (defined by normal and tangential components, δ_n and δ_s, respectively) with the traction vector acting on it (defined by the normal and tangential components, t_n and t_s) [25]. The initial response is linear with an elastic stiffness of $K = 5.0 \times 10^7$ MPa/mm, which is large enough to ensure the displacement continuity at the interface and to avoid any modification of the stress fields around the fibers in the absence of damage. The linear behavior ends at the onset of damage, which is dictated by a maximum stress criterion expressed mathematically as

$$max\left\{\frac{\langle t_n \rangle}{N}, \frac{t_s}{S}\right\} = 1 \tag{5}$$

where N and S stand for interface strength in tension and shear, respectively [17]. Once the damage begins, the stress transferred through the crack is reduced depending on the interface damage parameter d, which evolves from 0 (in the absence of damage) to 1 (no stresses transmitted across the interface). The corresponding traction-separation law is expressed by

$$t_n = (1-d)K\delta_n \quad \text{if} \quad \delta_n > 0$$

$$t_s = (1-d)K\delta_s \tag{6}$$

The evolution of the damage parameter is controlled by an effective displacement, $\bar{\delta}$, defined as the norm of the displacement jump vector across the interface as

$$\bar{\delta} = \sqrt{<\delta_n>^2 + \delta_s^2}, \tag{7}$$

and d depends on the maximum effective displacement at the interface attained during the loading history at each material integration point $\bar{\delta}^{max}$ according to

$$d = \frac{\bar{\delta}^f(\bar{\delta}^{max} - \bar{\delta}^0)}{\bar{\delta}^{max}(\bar{\delta}^f - \bar{\delta}^0)} \tag{8}$$

where $\bar{\delta}^0$ and $\bar{\delta}^f$ stand for the effective displacement at the onset of damage ($d = 0$) and when the interface has failed completely ($d = 1$), respectively.

The mechanical response of the interface is controlled by the normal (N) and shear (S) interface strength and by the energy necessary to completely break the interface, G_{int}, (which is independent of the loading path in this model). The shear interface strength $S = 75$MPa was measured by means of indentation push-out experiments carried out in thin slices of the composite material [17]. The normal strength $N = 100$ MPa and the interface fracture energy $G_{int} = 10$ J/m^2 were calibrated by means of computational micromechanics simulations of representative volume element of the composite in tension. More details about the cohesive crack model implementation can be found in [25, 20].

Finally, the 0° layers with the fiber aligned in the loading direction were assumed to be linear elastic. Their thermo-elastic constants (elastic moduli parallel and perpendicular to the fibers, E_1 and E_2, coefficients of thermal expansion parallel and perpendicular to the fibers, α_1 and α_2 and the in-plane Poisson's ratio and shear modulus, ν_{12} and G_{12}) were obtained from the matrix and fiber properties and volume fraction (65%) using the Mori-Tanaka mean-field approximation [26] and they can be found in Table 2 for

the AS4 carbon/epoxy and E glass/epoxy plies. Simulations were carried out under generalized plane strain conditions using Abaqus/Standard and within the framework of the small deformations theory.

3. Results

Numerical simulations of the four RVEs in Figure 2 were carried out to assess the influence of the transverse layer thickness on the onset and propagation of through-thickness cracks. The 2D model cannot take into account the crack propagation along the fiber direction (tunneling) and it is appropriate to simulate transverse cracking of thick plies, which is controlled by Y_T^{tt} according to equation (1). Simulations were performed in two steps. Firstly, the RVE was subjected to a homogeneous temperature change of ΔT = -100°C to generate the thermal residual stresses that develop after curing upon cooling to ambient temperature. No initial damage in the matrix or at the fiber/matrix interface was found after this step. Afterwards, tensile deformation was applied by increasing the displacement δ_x, leading to the progressive cracking of the 90° layer.

3.1. First microcrack

The initial deformation of the RVE was elastic but the stress field within the RVE was inhomogeneous. The onset and propagation of the first crack in the 90° ply is depicted in Figs. 4(a) and (b) for the carbon/epoxy cross-ply laminates with the thinnest ($[0_2/90/0_2]$) and thickest ($[0_2/90_8/0_2]$) 90° ply. Damage started by interface decohesion in one fiber and propagated very rapidly along the interface of neighbor fibers in the thin ply, leading to the formation of a thin crack through-the-thickness of the 90° ply, Fig. 4(a). Crack initiation in thick 90° plies was also triggered by matrix/fiber decohesion close to the interface between 0° and 90° plies, Fig. 4(b). As the applied strain increased, damage in the form of interface decohesion and shear matrix failure between debonded fibers propagated across the ply. The actual crack path depended on the fiber distribution leading to significant crack branching and meandering in the through-thickness crack. The differences between the thin cracks in thin 90° plies and the wider damage zone in thick 90°, accompanied by crack branching and the formation of oblique cracks

are in very good agreement with experimental observations in the literature [17, 27, 28, 29]. Similar results were obtained for E glass/epoxy laminates and they are not included for sake of brevity.

3.2. Transverse ply strength

The strength of the 90° ply, understood as the maximum stress carried by the transverse ply during deformation, can be computed from the total force per unit width carried by the laminate, P, minus the contribution of the 0° plies, that are assumed to be linear elastic. Accordingly, the stress on the 90° ply, σ_x, under plane strain conditions is given by

$$\sigma_x = \frac{P - \epsilon_x t_0 \frac{E_1}{(1-\nu_{12}\nu_{21})}}{t_{90}} + \sigma_x^{th} \tag{9}$$

where ϵ_x is the mechanical strain (computed from the applied displacement along the loading direction after cooling down at ambient temperature), σ_x^{th} the thermal residual stress in the 90° ply along the x direction after cooling down upon ambient temperature and t_0 and t_{90} stand for the thickness of the 0° and 90° plies, respectively. The thermal residual stress, σ_x^{th} is given by

$$\sigma_x^{th} = \epsilon_x^{th} \frac{E_2}{(1 - \nu_{12}\nu_{21})} \tag{10}$$

where ϵ_x^{th} is the corresponding thermal residual strain in the 90° ply after cooling down upon ambient temperature.

This definition of the ply strength has two advantages: it can be easily determined from experimental results and it does not require to ascertain whether the first matrix crack has propagated through the whole thickness of the ply, a task that may be very difficult in very thin plies because of the reduced crack opening displacement of transverse cracks [29]. Nevertheless, it should be noted that eq. (9) implicitly assumes –following the postulates of the classical laminate theory– that the stress in the 0° plies is constant and does not take into account the local load transfer from the 90° ply to the 0° as a result of the development of a transverse crack. Although this

contribution to the total load carried by the 0° is very small, it can be of the same order of magnitude that the total load carried by the 90° ply and cannot be neglected in this analysis. One advantage of the computational micromechanics approach presented in this paper is that the stress carried by the 90° ply can be computed from the results of the finite element analysis using eq. (9) but it can also be determined as the average stress carried by the 90° ply, $\overline{\sigma}_x$, obtained by numerical integration of the stress in the x direction in the whole transverse ply according to

$$\overline{\sigma}_x = \frac{\sum_i \sigma_x^i \Omega^i}{\sum_i \Omega^i} \tag{11}$$

where σ_x^i and Ω^i stand, respectively, for the stress in the x direction and the area associated to the Gauss point i in the whole finite element discretization of the 90° ply.

The transverse ply strength, Y_T^{tt} has been plotted as a function of the transverse ply thickness in Figs. 5(a) and (b) for the carbon/epoxy and glass/epoxy cross-ply laminates, respectively. The results for the ply strength obtained from classical laminate theory (eq. 9) and computational micromechanics (eq. 11) are plotted together with the broken horizontal line that is the prediction for the *in situ* transverse strength of thick plies according to Dvorak and Laws [10], eq. (3). In this equation, the transverse tensile strength of an unconstrained unidirectional ply, Y_T, was computed by means of computational micromechanics through the finite element analysis of a square RVE of the microstructure of the composite subjected to transverse tension with periodic boundary conditions [30]. These simulations were carried out using the fiber volume fraction as well as the matrix, fiber and interface properties of both the AS4 and the E glass fiber/epoxy composites. The results of computational micromechanics, that provide the actual strength of the transverse ply, demonstrated that there is not size effect on the stress necessary to initiate a transverse crack through the laminate thickness, in agreement with the fracture mechanics postulates. Moreover, the approximation of Dvorak and Laws [10], eq. (3), for the *in situ* strength tends to overestimate slightly the actual transverse strength but it can be considered fairly accurate for both carbon and glass fiber composites.

The computational micromechanics simulations showed that the trans-

verse ply strength of carbon fiber composites was $\approx$ 25 MPa higher than that of glass fiber composites. This difference in the transverse strength has to be attributed to the differences between the carbon and glass fiber elastic modulus, as the matrix and interface properties as well as the fiber volume fraction were identical in both cases. Transverse cracking was triggered by interface decohesion and this mechanism developed earlier in the glass fiber composite because the elastic stress concentration at the fiber/matrix interface was enhanced by the high modulus mismatch between the glass fiber (74 GPa) and the epoxy matrix (3.5 GPa). On the contrary, the transverse elastic modulus of the AS4 carbon fiber (13 GPa) was much closer to that of the matrix, and the stress concentration at the interface weaker.

Interestingly, the ply strength computed from classical laminate theory is higher than the actual ply strength obtained by averaging the stress in the transverse ply and predicts a size effect in the case of carbon / epoxy composites. The differences between both can be understood from Fig. 6 in which the distribution of σ_x is plotted across a section of the laminate in which damage has developed in the transverse ply. Figs. 6(a) and (b) correspond to $[0_2/90_2/0_2]$ carbon/epoxy and glass/epoxy laminates, respectively The load shed by the transverse ply as soon as damage starts near to the 0/90 ply interface leads to the development of a stress concentration in the 0° ply. Classical laminate theory assumes that the load carried by the 0° plies is constant (the broken line in Fig. 6 and the extra load carried by these plies due to the stress concentrations is assigned to the 90° ply, overestimating the strength of the transverse ply. The effect increases with the elastic mismatch between E_1 and E_2 and also as the thickness of the transverse ply decreases. It was maximum and led to a noticeable size effect in the case of carbon/epoxy composites for which $E_1/E_2 = 15.3$ and very limited for glass /epoxy composites with $E_1/E_2 = 3.1$.

3.3. Multiple Microcracking

Further straining after the first matrix crack led to development of multiple matrix cracks along the 90° ply. The evolution of the cracking pattern with the applied strain is shown in Figure 7a for the $[0_2/90_4]_s$ laminate. Matrix cracks are evenly distributed along the ply as the stress relief around each crack impedes the development of new cracks in the vicinity of old cracks. The numbers of cracks per unit length, i.e. the crack density, depended on

the ply thickness. This is shown in Figure 7b in which the crack pattern at the end of the simulations is depicted for the different laminates. It should be noted that simulations stopped before the maximum crack density was attained due to convergency problems.

The evolution of the crack density in the transverse ply with the applied strain in the carbon/ epoxy and glass/epoxy $[0_2/90_{1/2}]_s$ cross-ply laminates is plotted in Fig. 8. The crack density *vs.* strain curve presented a sigmoidal shape, in agreement with the experimental results [5]: the number of cracks per unit length increased linearly with the applied strain after the development of the first matrix crack but the development of new matrix cracks slowed down as the strain increased.

The predictions for the degradation of the elastic modulus of the transverse ply, $E_x^{90^\circ}$ (normalized by the initial modulus $E_{x0}^{90^\circ}$), obtained by computational micromechanics are plotted in Figs. 9(a) and (b) for the carbon/epoxy and glass/epoxy cross-ply laminates, respectively. The elastic modulus of the transverse ply was computed as the average stress carried by the ply along the x axis, given by equation (11), divided by the total strain $(\epsilon_x + \epsilon_x^{th})$. The degradation of the elastic modulus with the applied strain began earlier in the glass/epoxy laminates, because of the early cracking as a result of the elastic modulus mismatch between matrix and fibers, and progressed rapidly afterwards. No influence of the transverse ply thickness on the reduction of the elastic modulus was found among the thicker laminates. Nevertheless, the reduction of the modulus with the applied strain was more limited in the thinnest ply.

4. Concluding remarks

The development of transverse ply cracking during tensile deformation of cross-ply laminates was studied by means of computational micromechanics. In this strategy, the longitudinal 0° plies were represented by homogeneous, anisotropic elastic solids while the actual fiber dispersion in the matrix was included in the model of the transverse 90° plies. The mechanical response of the laminate was simulated by means of the finite element analysis under plane strain of an elongated RVE of the laminate with periodic boundary conditions. Both fiber/matrix interface decohesion as well as matrix failure

were taken into account in the simulations. The emphasis was placed in the initiation and propagation of through-thickness cracks as crack propagation along the fibers (tunneling) would require a full 3D model.

This strategy was used to study the influence of the ply thickness on the onset and development of cracking in carbon/epoxy and glass/epoxy cross-ply laminates of the family $[0_2/90_{n/2}]_s$ with $n = 1$, 2, 4, and 8. It was found that transverse matrix cracking was always triggered by interface decohesion and leading to the formation of a dominant crack propagated from the interface between 0 and 90 plies towards the center of the ply. Upon further deformation, damage localized in one single crack that spanned the whole thickness of the 90° ply and the first transverse crack was developed. The actual crack path depended on the fiber distribution leading to significant crack branching and meandering in the through-thickness crack for thick laminates, in agreement with the experimental evidence.

It was found that the transverse ply strength corresponding to the initiation and propagation of a through-thickness crack was independent of the ply thickness, in agreement with the postulates of fracture mechanics. The transverse strength of carbon/epoxy laminates was 35% higher than that of the glass fiber counterparts because of the reduced elastic modulus mismatch between matrix and fiber in the transverse direction. In addition, the approximation of Dvorak and Laws [10], eq. (3), for the *in situ* ply strength was fairly accurate for both carbon and glass fiber composites. The progressive cracking of the transverse plies was also simulated and the variation of the crack density with the applied strain presented a sigmoidal shape, in agreement with the results in the literature [5].

Finally, the actual potential of this computational micromechanics framework to explore the influence of matrix, fiber and interface properties (elastic constants, strength, toughness) on the development of transverse matrix cracking in multiaxial laminates should be highlighted. Moreover, the detailed information on the nucleation and growth of damage can lead to improved microstructural design strategies to enhance the resistance to transverse cracking and will help to improve the accuracy of current models based on the homogenized ply properties to predict cracking as well as damage. These possibilities will be exploited in future investigations.

5. Acknowledgments

The authors kindly acknowledge the support of the Spanish Ministry of Economy and Competitiveness through the project MAT2012-37552. CSL acknowledges the support of the Spanish Ministry of Economy and Competitiveness through the Ramon y Cajal program.

[1] J. Nairn, Matrix microcracking in composites, in: R. Talreja, J. A. Manson (Eds.), Comprehensive Composite Materials, Vol 2,, Elsevier Science, 2000, pp. 403–432.

[2] R. Talreja, C. Singh, Damage and Failure of Composite Materials, Cambridge Press, 2012.

[3] A. Parvizi, K. W. Garret, J. E. Bailey, Constrained cracking in glass fibre-reinforced epoxy cross-ply laminates, Journal of Material Science 13 (1978) 195–201.

[4] A. Parvizi, J. E. Bailey, Multiple transverse cracking in glass-fiber epoxy cross-ply laminates, Journal of Material Science 13 (1978) 2131–2136.

[5] F. W. Crossman, W. J. Warren, A. S. D. Wang, J. G. E. Law, Initiation and growth of transverse cracks and edge delamination in composite materials: Part 2. Experimental correlation, Journal of Composite Materials 14 (1980) 89–108.

[6] D. L. Flaggs, M. H. Kural, Experimental determination of the in situ transverse lamina strength in graphite/epoxy, Journal of Composite Materials 16 (1982) 103–116.

[7] K. Kawabe, T. Matsuo, Z. Maekawa, New technology for opening various reinforcing fiber tows, Journal of the Society of Materials Science, Japan 47 (1998) 727–734.

[8] S. Sihn, R. Y. Kim, K. Kawabe, S. Tsai, Experimental studies of thin-ply laminated composites, Composite Science and Technology 67 (2007) 996–1008.

[9] H. Saito, H. Takeuchi, I. Kimpara, A study of crack suppression mechanism of thin-ply carbon-fiber-reinforced polymer laminate with mesoscopic numerical simulation, Journal of Composite Materials 48 (2014) 2085–2096.

[10] G. Dvorak, N. Laws, Analysis of progressive matrix cracking in composite laminates ii. first ply failure, Journal of Composite Materials 21 (1987) 309–329.

[11] P. P. Camanho, C. G. Dávila, S. T. Pinho, L. Iannucci, P. Robinson, Prediction of in situ strengths and matrix cracking in composites under transverse tension and in-plane shear, Composites: Part A 37 (2006) 165–176.

[12] F. P. van der Meer, C. G. Dávila, Cohesive modeling of transverse cracking in laminates under in-plane loading with a single layer of elements per ply, International Journal of Solids and Structures 50 (2013) 3308–3318.

[13] C. González, J. LLorca, Mechanical behavior of unidirectional fiber-reinforced polymers under transverse compression: microscopic mechanisms and modeling, Composites Science and Technology 67 (2007) 2795–2806.

[14] E. Totry, J. M. Molina-Aldareguía, C. González, J. LLorca, Effect of fiber, matrix and interface properties on the in-plane shear deformation of carbon-fiber reinforced composites, Composites Science and Technology 70 (2010) 970–980.

[15] C. González, J. LLorca, Multiscale modeling of fracture in fiber-reinforced composites, Acta Materialia 54 (2006) 4171–4181.

[16] C. González, J. LLorca, Virtual fracture testing of fiber-reinforced composites: A computational micromechanics approach, Engineering Fracture Mechanics 74 (2007) 1126–1138.

[17] L. P. Canal, C. González, J. Segurado, J. LLorca, Intraply fracture of fiber-reinforced composites: microscopic mechanisms and modeling, Composites Science and Technology 72 (2012) 1223–1232.

[18] J. LLorca, C. González, J. M. Molina-Aldareguía, J. Segurado, R. Seltzer, F. Sket, M. Rodríguez, S. Sádaba, R. Muñoz, L. P. Canal, Multiscale modeling of composite materials: a roadmap towards virtual testing, Advanced Materials 23 (2011) 5130–5147.

[19] J. Segurado, J. LLorca, A numerical approximation to the elastic properties of sphere-reinforced composites, Journal of the Mechanics and Physics of Solids 50 (2002) 2107–2121.

[20] Abaqus Standard, Version 6.13. Dassault Systemes, Simulia.

[21] M. Rodríguez, J. M. Molina-Aldareguía, C. González, J. LLorca, Determination of the mechanical properties of amorphous materials through instrumented nanoindentation, Acta Materialia 60 (2012) 3953–3964.

[22] C. S. Lopes, P. P. Camanho, Z. Gürdal, P. Maimí, E. V. González, Low-velocity impact damage on dispersed stacking sequence laminates. Part II: Numerical simulations, Composites Science and Technology 69 (2009) 937–947.

[23] J. Lee, G. Fenves, Plastic-damage model for cyclic loading of concrete structures, Journal of Engineering Mechanics 124 (1998) 892–900.

[24] J. Lubliner, J. Oliver, S. Oller, E. Oate, A plastic-damage model for concrete, International Journal of Solids Structures 25 (1989) 299–326.

[25] P. Camanho, C. G. Dávila, Mixed-mode decohesion finite elements for the simulation of delamination in composite materials, NASA/TM-2002-211737, 2002.

[26] Y. Benveniste, A new approach to the application of Mori-Tanaka's theory in composite materials, Mechanics of Materials 6 (1987) 147–157.

[27] M. Jalalvand, M. R. Wisnom, H. Hosseini-Toudeshky, B. Mohammadi, Experimental and numerical study of oblique transverse cracking in cross-ply laminates under tension, Composites Part A 67 (2014) 140–148.

[28] T. A. Sebaey, J. Costa, P. Maimí, Y. Batista, N. Blanco, J. A. Mayugo, Experimental evaluation of the damage growth restraining in 90° layer

of thin-ply cfrp cross-ply laminates, Advanced Composite Materials 21 (2012) 57–66.

[29] T. A. Sebaey, J. Costa, P. Maimí, Y. Batista, N. Blanco, J. A. Mayugo, Measurement of the in situ transverse tensile strength of composite plies by means of the real time monitoring of microcracking, Composites Part B 65 (2014) 40–46.

[30] L. P. Canal, J. Segurado, J. LLorca, Failure surface of epoxy-modified fiber-reinforced composites under transverse tension and shear, International Journal of Solids and Structures 46 (2009) 2265–2274.

Table 1: Parameters that control the mechanical properties of the epoxy matrices.

Epoxy	E_m (GPa)	ν_m	α_m ($10^{-6}\mathrm{K}^{-1}$)	σ_m^c (MPa)	α_{ps}	σ_m^t (MPa)	G_m ($\mathrm{J/m^2}$)
8552	5.1	0.35	52	176	0.18	121	90
MTM57	3.5	0.35	50	105	0.13	75	100

Table 2: Homogenized ply properties according to the Mori-Tanaka model [26].

Ply	E_1 (GPa)	E_2 (GPa)	ν_{12}	G_{12} (GPa)	α_1 ($10^{-6}\mathrm{K}^{-1}$)	α_2 ($10^{-6}\mathrm{K}^{-1}$)
AS4 Carbon/epoxy	141	9.2	0.32	4.8	-0.34	34.4
E Glass/epoxy	45.7	14.5	0.25	4.5	6.2	28.9

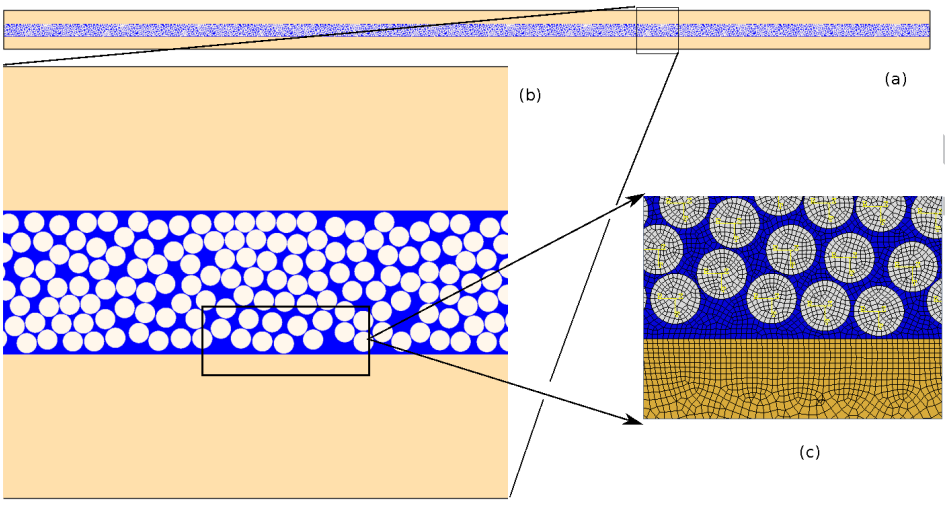

Figure 1: (a) RVE of the composite laminate with stacking sequence $[0_2/90]_s$. (b) Detail of the 90° ply, showing the fiber distribution within the ply. (c) Detail of the fiber distribution at the interface between 0° and 90° plies as well as of the finite element discretization.

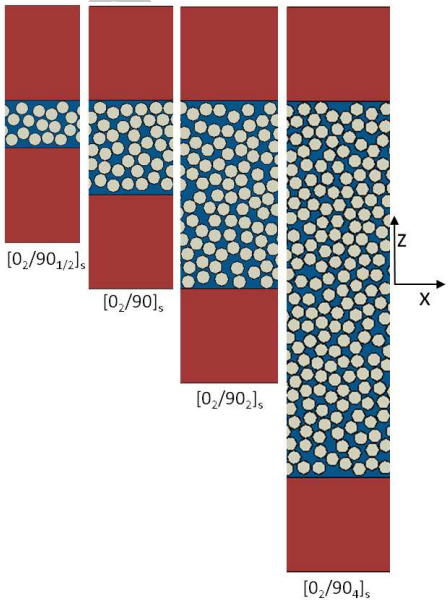

Figure 2: Central slices of the different RVEs of the $[0_2/90_{n/2}]_s$. (n = 1, 2, 4 and 8).

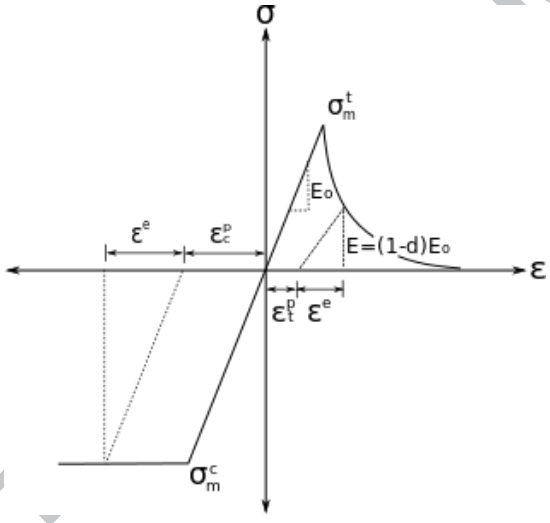

Figure 3: Schematic of the uniaxial tension-compression response of the epoxy matrix according to the damage-plasticity model for quasi-brittle materials.

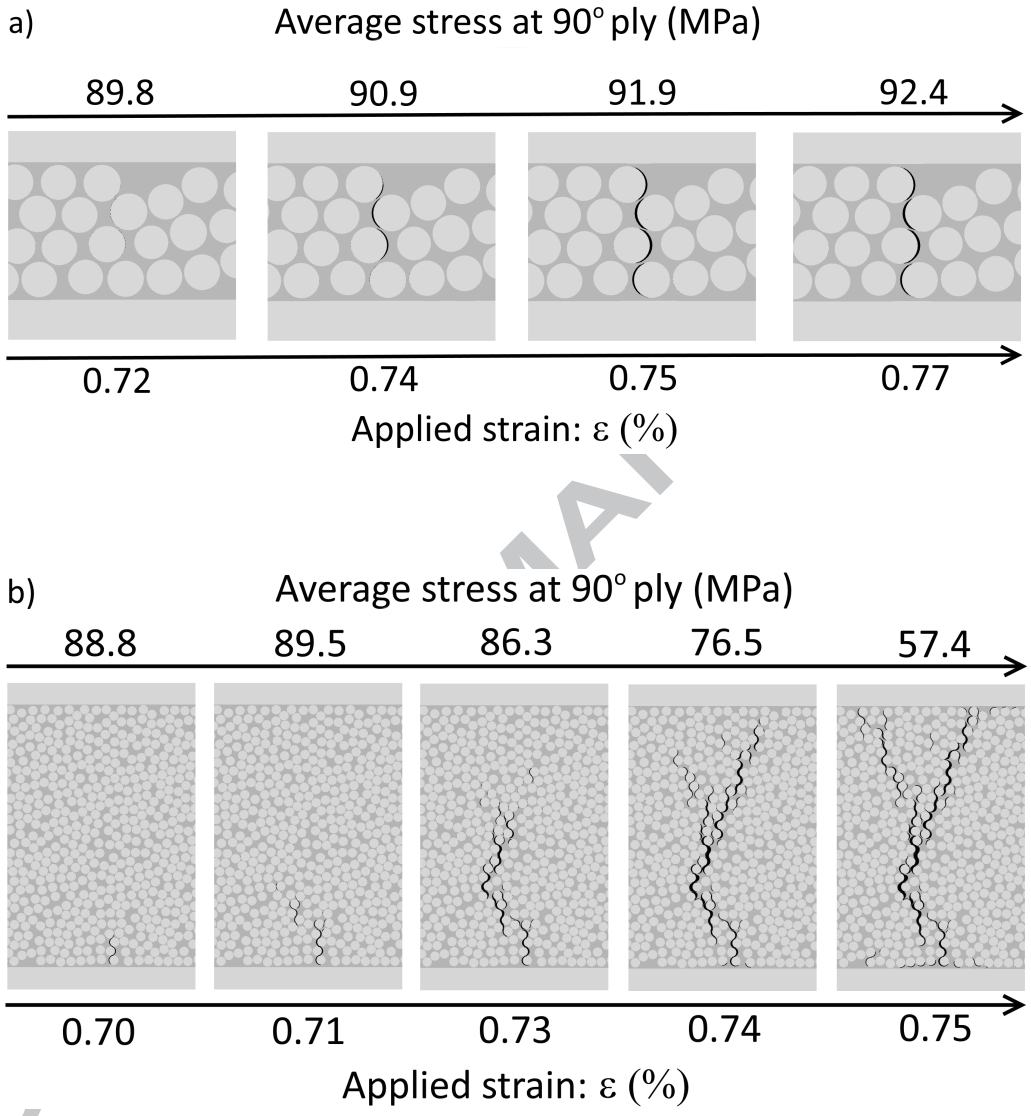

Figure 4: Development of the first matrix crack in the 90° ply of the carbon/epoxy cross-ply laminates. (a) $[0_2/90/0_2]$ laminate. (b) $[0_2/90_8/0_2]$ laminate. The mechanical strain (computed from the applied displacement after cooling at ambient temperature) and the stress in the loading direction on the 90° ply (computed from eq. (10)) are shown above and below each plot, respectively. See text for details.

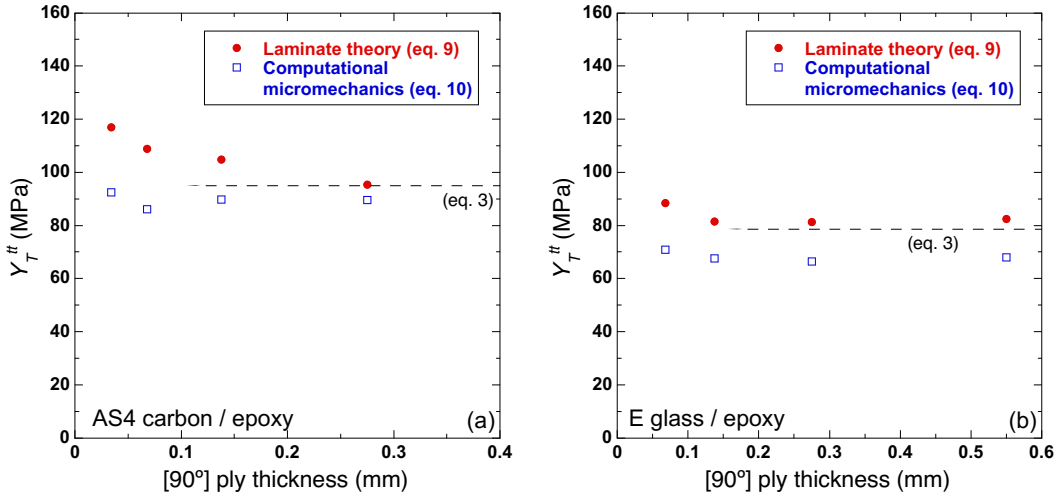

Figure 5: Transverse ply strength , Y_T^{tt}, as a function of the transverse ply thickness. (a) AS4 carbon /epoxy cross-ply laminate. (b) E glass / epoxy cross ply laminate. The predictions from laminate theory (eq. 9), computational micromechanics (eq. 10) and from the *in situ* transverse strength for thick plies (eq. 3) are included in each plot.

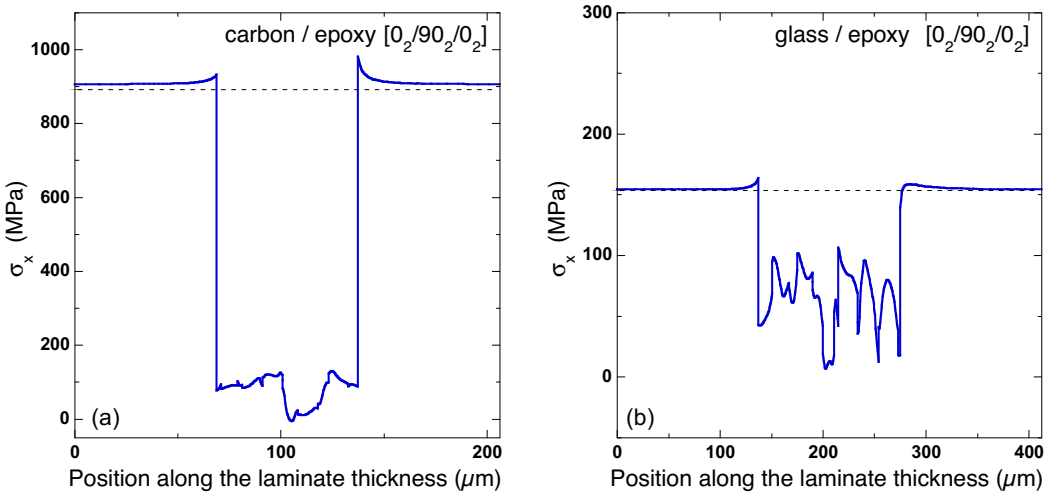

Figure 6: Variation of σ_x across one section of the cross-ply laminate for a given strain in which damaged has developed in the transverse ply. (a) Carbon / epoxy $[0_2/90_2/0_2]$, ϵ_x = 0.64%. (b) Glass / epoxy $[0_2/90_2/0_2]$, ϵ_x = 0.35%. The broken line in each plot stands for the stress carried by the 0° plies according to the classical laminate theory.

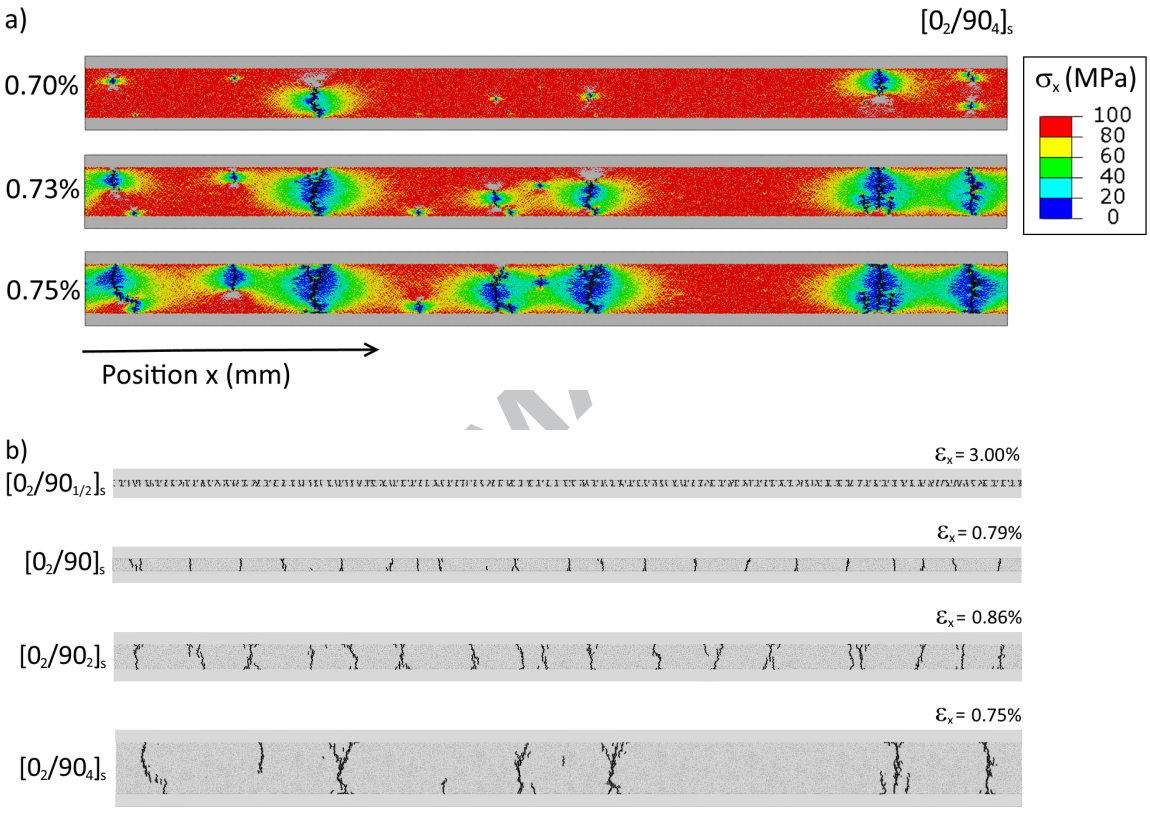

Figure 7: a) Evolution of the cracking pattern with the applied strain in the $[0_2/90_4]_s$ carbon/epoxy laminate. The contour plots of σ_x show the stress relief around the cracks. b) Final cracking pattern at the end of the simulation for the different laminate configurations analyzed $[0_2/90_{n/2}]_s$. The corresponding applied strain is indicated for each laminate.

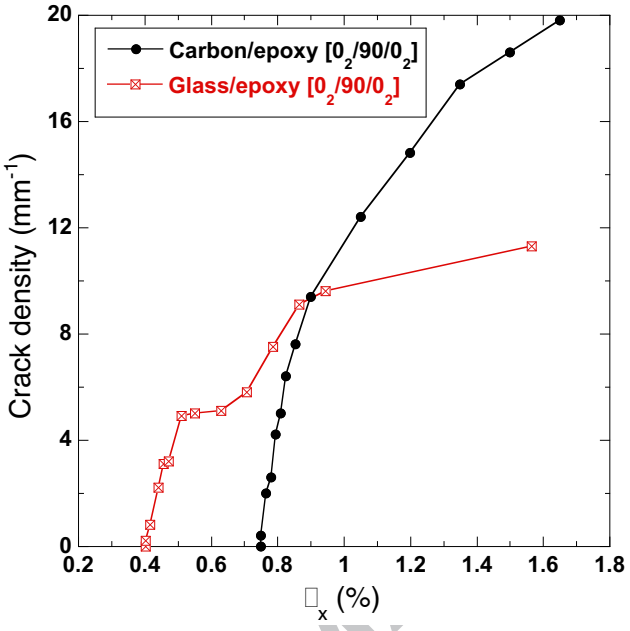

Figure 8: Evolution of the crack density in the transverse ply with the applied strain in the carbon/ epoxy and glass/epoxy $[0_2/90_{1/2}]_s$ cross-ply laminates.

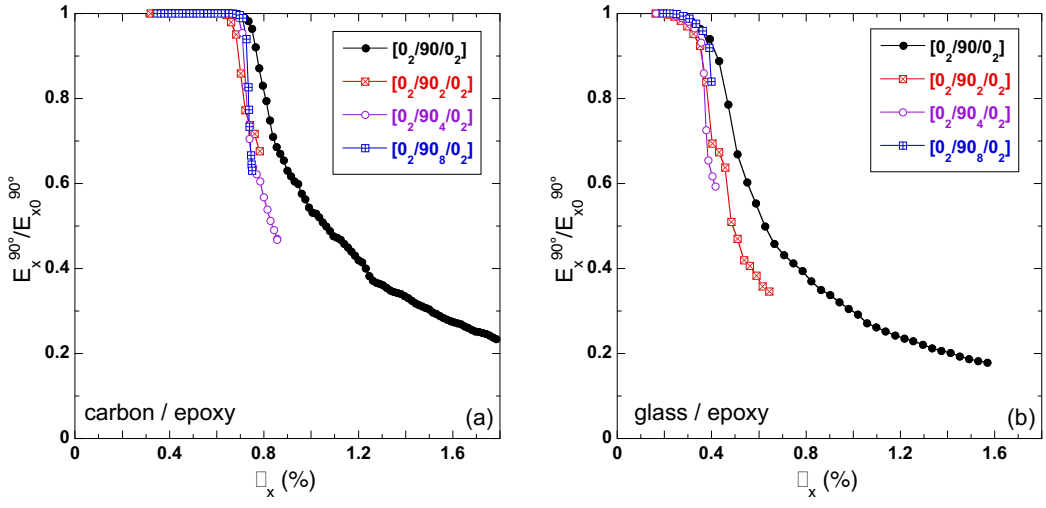

Figure 9: Evolution of the elastic modulus in the transverse ply, $E_x^{90^\circ}$, (normalized by the initial elastic modulus $E_{x0}^{90^\circ}$) with the applied strain. (a) Carbon/ epoxy cross-ply laminates. (b) Glass/epoxy cross-ply laminates